Volume 1 | Number 1 | Jan 2013 | Pages 1–100

Dalton Transactions

An international journal of inorganic chemistry
www.rsc.org/dalton

ROYAL SOCIETY OF CHEMISTRY

ROYAL SOCIETY OF CHEMISTRY

www.rsc.org/dalton

D_{5h} [PhSiO$_{1.5}$]$_{10}$ Synthesis via F$^-$ Catalyzed Rearrangement of [PhSiO$_{1.5}$]$_n$. An Experimental/Computational Analysis of Likely Reaction Pathways.

Joseph C. Furgal,[1] Theodore Goodson III,[*1,2] Richard M. Laine[*2,3]

Chemistry,[1] Macromolecular Sci. and Eng. Center,[2] and Materials Sci. and Eng.[3] Depts., University of Michigan, Ann Arbor, MI 48109-2136.

Abstract

We describe here the synthesis and analysis of the reaction pathways leading to formation of the rare D_{5h} decaphenylsilsesquioxane (SQ) [PhSiO$_{1.5}$]$_{10}$ via F$^-$ catalyzed rearrangement of [PhSiO$_{1.5}$]$_n$ n = 8, 12, and oligomers initially synthesized from PhSi(OEt)$_3$. Isolated yields of ~50% [PhSiO$_{1.5}$]$_{10}$ are obtained via rearrangement of all starting materials. The recovered starting materials can be re-equilibrated using catalytic F$^-$ to generate similar yields in second batches. These yields arise because [PhSiO$_{1.5}$]$_{10}$ exhibits higher solubility and better energy stabilization (10 kcal/mol theory) in CH$_2$Cl$_2$ compared to [PhSiO$_{1.5}$]$_8$ or [PhSiO$_{1.5}$]$_{12}$. Reaction intermediates were identified using time dependent ^{19}F NMR and MALDI-ToF mass spectrometry eventually equilibrating to form the 8:10:12 cages in a 1:3:1.3 equilibrium in CH$_2$Cl$_2$.

Experimental results coupled with modeling using the Gamess computational package provide multiple reasonable pathways for SQ rearrangements to [RSiO$_{1.5}$]$_{10}$, starting from [RSiO$_{1.5}$]$_8$. Heats of reaction for interconversion of the model intermediates [HSiO$_{1.5}$]$_x$ determined computationally, were used to select the *most reasonable reaction pathways*. The findings support a mechanism involving activation and cleavage of a T$_8$ cage corner by F$^-$ attachment, followed by the corners stepwise removal as [i.e. RSi(OH)$_3$], followed thereafter by reinsertion forming [RSiO$_{1.5}$]$_9$-OH followed by, insertion of another corner to form [RSiO$_{1.5}$]$_{10}$-(OH)$_2$ and finally condensation to give [RSiO$_{1.5}$]$_{10}$. The most enthalpically favorable path (-24 kcal/mol) involves a hybrid mechanism.

Introduction

Silsesquioxanes (SQs) are of considerable recent interest due to their potential to offer high degrees of functionalization, high thermal stability, and simple purification. To date there have been some 18 reviews on silsesquioxane based materials, with most focusing on T_8 (O_h) compounds.[1-18] However, higher order SQs such as T_{10} (D_{5h}) and T_{12} (D_{2d}) are of increasing interest, since they offer new geometries, higher potential degrees of functionalization, and in many cases superior solubilities. [13,17,19-21] They also offer similar but not identical thermal stabilities and physical properties to T_8.

Most SQ syntheses rely on hydrolysis and condensation of R_1SiCl_3 or $R_1Si(OR')_3$.[2] These reactions often suffer from low yields, < 30%, can take weeks to months to reach completion, and coincidentally produce $[RSiO_{1.5}]_n$ byproducts that until recently were simply discarded. The $[PhSiO_{1.5}]_n$, n = 8,10,12, systems are particularly amenable for post synthetic modification using traditional electrophilic aromatic substitution methods.[17,22]

$[PhSiO_{1.5}]_8$ or OPS, the most frequently studied, was first synthesized by Barry et al. in 1955.[23] Multiple synthetic routes to $[PhSiO_{1.5}]_8$ have been reported,[13,17,24,25] whereas only a couple of reports describe the synthesis of $[PhSiO_{1.5}]_{12}$.[21,24] A typical route to T_8 involves refluxing $PhSi(OEt)_3$ in toluene with KOH under water scarce conditions for < 48 h to give 90^+ % yields.[17,24] $[PhSiO_{1.5}]_{12}$ can be made similarly, with THF instead of toluene (~50% yield).[13,24]

Unfortunately, there are no simple, high yield routes to pure five-fold symmetric $[PhSiO_{1.5}]_{10}$.[24-37], Brown et al. first isolated $[PhSiO_{1.5}]_{10}$ in 1963 with an unreported yield, as the most soluble component after fractionation of crude $[PhSiO_{1.5}]_8$ by refluxing in benzene/hexane.[24] We previously synthesized $[PhSiO_{1.5}]_{10}$ using 18-crown-6/BaO to catalytically equilibrate 3 g of $[PhSiO_{1.5}]_{12}$ in m-xylene, giving only 500 mg [15% yield] after repeated recrystallization.[26] This method provided crystals suitable for single crystal x-ray diffraction.

Our recent synthetic efforts have explored the efficacy of using fluoride as nBu_4NF (TBAF) to catalyze the synthesis of SQs containing electron withdrawing R-groups (i.e. phenyl, vinyl), with recovered yields as high as 99%.[27-32] For example we have made mixed functional SQ intermediates for "beads on a chain" (BoC) polymers; SQ cages connected with organic linkers, with mixed $T_{10/12}$ vinyl/Me and mixed $T_{10/12}$ vinyl containing SQs.[27,29,31-32] Motivation for our initial work comes from studies by Bassindale et al. and Mabry and Bowers et al. who found that

SQs will react with stoichiometric TBAF (or Me_4NF, TMAF) forming cages that encapsulate F^- (F^- @$[RSiO_{1.5}]_8$) on slow evaporation of dry THF solution.[38-42]

Bassindale et al. also explored F^- catalyzed syntheses of T_8 cages from $RSi(OR')_3$.[39] They compared the activity of anhydrous F^- with F^- + ^{18}O labeled water, finding that cage formation depends strongly on water concentration, similar to what is observed in standard hydrolysis/condensation conditions using strong acids/bases. This is expected since $RSi(OR')_3$ hydrolysis is a necessary first step before condensation.

Further motivation comes from Kawakami et al. who used TBAF to catalyze formation of 4-TMS-$PhSiO_{1.5}]_{8,10,12}$ derivatives from 4-TMS-$PhSi(OEt)_3$.[33] The [4-TMS-$PhSiO_{1.5}]_{8,10,12}$ cages were then nitrated forming [4-NO_2-$PhSiO_{1.5}]_{8,10,12}$ and the individual cages isolated by selective crystallization.

Our objectives in the studies reported here are to develop a mechanistic picture of the processes that occur in F^- catalyzed rearrangement of $[PhSiO_{1.5}]_{8/12}$, $PhSi(OEt)_3$, and the $[PhSiO_{1.5}]_n$ by-products with the goal of optimizing the synthesis of $[PhSiO_{1.5}]_{10}$. Optimization was necessary to generate $[PhSiO_{1.5}]_{10}$ in sufficient quantities to permit further functionalization e.g. bromination, iodination, acylation, sulfonylation, alkylation, etc.[17,26,34,43] Scheme **1** depicts the general conditions for F^- catalyzed synthesis of $[PhSiO_{1.5}]_{8,10,12}$.
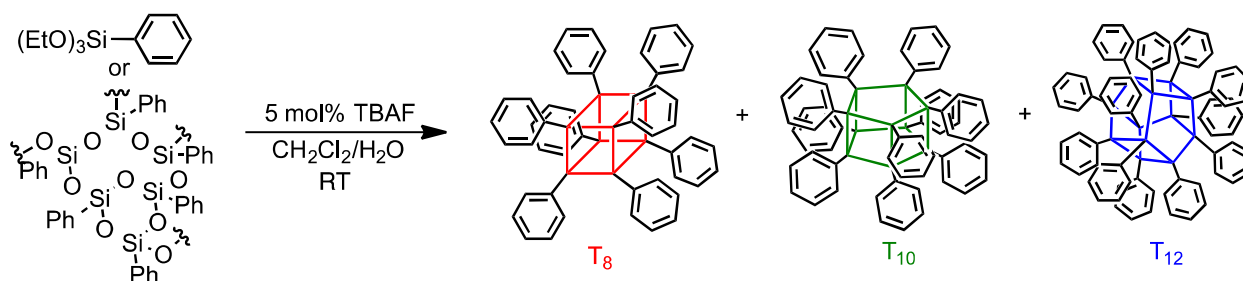
Scheme 1. Synthesis of $[PhSiO_{1.5}]_{8,10,12}$ by F^- catalyzed rearrangement.

The mechanism(s) of SQ cage formation even for the widely studied $[RSiO_{1.5}]_8$ compounds is(are) largely unknown, however Kudo and Gordon in a comprehensive modeling study developed a detailed picture of "reasonable" routes to T_8 cage formation via hydrolysis/condensation reactions of $HSiO(OH)_3$. Their studies suggest a very complex set of equilibria including more than 25 possible intermediates.[44-47] In short, cage formation is initiated by formation of D_4 rings that then self-condense. Experimental support for this path finds that all cis $[PhSi(O)OH]_4$ rings form easily from $PhSi(OH)_3$. On standing at ambient, these rings self-condense to form OPS.[48,49]

Kudo and Gordon find that the presence of water promotes condensation of $HSi(OH)_3$ to $[HSiO_{1.5}]_8$ with a net heat of formation of -11.5 kcal/mol. In complementary work, Mashmeyer et al. also explored the cage formation mechanisms with the synthesis of incompletely condensed $[(c\text{-}C_5H_9)SiO_{1.5}]_7\text{-}(OH)_3$.[50] Reaction progress monitored via ESI mass spec and time dependent ATR-FTIR studies also suggest condensation mechanisms similar to those of Kudo and Gordon suggesting that $[(c\text{-}C_5H_9)SiO_{1.5}]_7\text{-}(OH)_3$ is a kinetic product. These studies provide the background for the work presented here.

The following sections discuss optimization of $[PhSiO_{1.5}]_{10}$ synthesis via a detailed analysis of the effects of variations in reaction conditions (i.e. concentration, solvent, catalyst, etc.), intermediates involved, and kinetic analyses of the synthetic process. This is followed by computational enthalpic/energy analysis of analogous $[HSiO_{1.5}]$ intermediates for the development of a potential mechanism for fluoride-catalyzed rearrangement of SQs.

Experimental
Materials and Analytical Methods

Materials were obtained by previously described methods or were purchased from commercial sources (see Supporting Information).[51] Products were characterized by typical characterization methods as described in SI including MALDI-ToF, (^{29}Si, ^{13}C and ^{1}H) NMR, TGA, GPC, and FTIR. Modeling studies were carried out using the Gamess software package.[52-53]

Synthesis

$[PhSiO_{1.5}]_{10}$ from $[PhSiO_{1.5}]_n$. To a 2 L round bottom flask under N_2 was added 16 g (124 mmol) $[PhSiO_{1.5}]_n$, ($[PhSiO_{1.5}]_8$ or polymeric resin), 1.75 L of methylene chloride, 5.2 mL (5.2 mmol) of 1 M TBAF in THF and magnetic stirrer. The reaction was stirred for 2-3 days at room temperature, or until the reaction mixture became transparent. The reaction was quenched with 50 g of powdered $CaCl_2$ and stirred for 1 day to remove the fluoride ion and then filtered through Celite. The solvent was then removed by rotary evaporation. The resulting white solid was then partially dissolved in 50 mL of a 1:1 THF:acetonitrile to selectively precipitate T_8 and T_{12} PhSQ. The resulting suspension of T_8 and T_{12} PhSQ was then filtered and reused in a subsequent synthesis. The solvent was then removed in-vacuo from the resulting solution containing T_{10} and partial cage PhSQ. It was then redissolved in a minimum amount of THF, precipitated into methanol to remove partial cages, filtered and dried under vacuum. $[PhSiO_{1.5}]_{10}$: white solid, 8.2 g, 52%.

Characterization Data: ^{1}H NMR (400 MHz, acetone-d6): δ7.31 (t, Ar-H), 7.45 (t, Ar-H), 7.68 (t, Ar-H) ppm; ^{13}C NMR: δ126.21, 126.54, 126.70, 127.31, 128.10, 128.64 ppm; ^{29}Si NMR (99 MHz, chloroform-d): 79.60 ppm; FTIR: 3066-2917 (νC-H), 1591(νC=C, Ar ring), 1429(νC=C, Ar ring), 1132 (νSi-O), 729 (νSi-C) cm^{-1}. MALDI-TOF: m/z (Ag$^+$ adduct) = 1399.8 [Ag-Si$_{10}$O$_{15}$(C$_6$H$_5$)$_{10}$]. GPC (found): Mn = 1.5 kDa, Mw = 2.4 kDa, PDI = 1.05. TGA (air, 10 °C/min 1000 °C): found 45.9%, calc 46.4%, T$_{d5\%}$: 489 °C.

Results and Discussion

In the following sections, we first discuss optimization of $[PhSiO_{1.5}]_{10}$ synthesis by F^- catalyzed rearrangement of $[PhSiO_{1.5}]_n$ via variations in experimental conditions and its characterization by MALDI-ToF, NMR, and TGA. This is followed by computational analyses of reaction intermediates (enthalpies). Lastly, we identify the multiple potential mechanistic pathways for the F^- catalyzed rearrangement of SQs and suggest the most likely reaction paths.

<u>Optimized Synthesis for $[PhSiO_{1.5}]_{10}$</u>

$[PhSiO_{1.5}]_{10}$ can be synthesized in high yield by F^- rearrangement of $[PhSiO_{1.5}]_n$ in dilute (~60 mM) CH_2Cl_2. This solvent system and concentration provides the highest selectivities/solubility for $[PhSiO_{1.5}]_{10}$ in the mixture of $[PhSiO_{1.5}]_{8,10,12}$ formed under these conditions. Reactions were typically run for 48 h to ensure full conversion of partial cages to completely condensed cages, starting from $PhSi(OEt)_3$, $[PhSiO_{1.5}]_n$, $[PhSiO_{1.5}]_{12}$ or $[PhSiO_{1.5}]_8$. Since this reaction results in a mixture of products, several steps are necessary to isolate pure $[PhSiO_{1.5}]_{10}$.

First, F^- must be removed as CaF_2 by treating the reaction solution with $CaCl_2$ or by washing with water as it will re-equilibrate all the cages if the isolated products are re-dissolved. Reactions were worked up using two methods. Aqueous extraction does work, but produces a higher proportion of hydroxyl containing partial cages that complicate further purification.[8,54] $CaCl_2$ quenching requires 24 h of stirring, but insoluble CaF_2 is removed easily by filtering and partial cage byproducts are minimal. This workup is the method of choice (Scheme **2**). The crude product mixture (before isolation) has a cage ratio: $T_8:T_{10}:T_{12}$ of ~1:3:1.3 by MALDI-ToF analysis (Figure **S1**). $T_{18,20,22}$ cage sizes were also observed and isolated as discussed below.
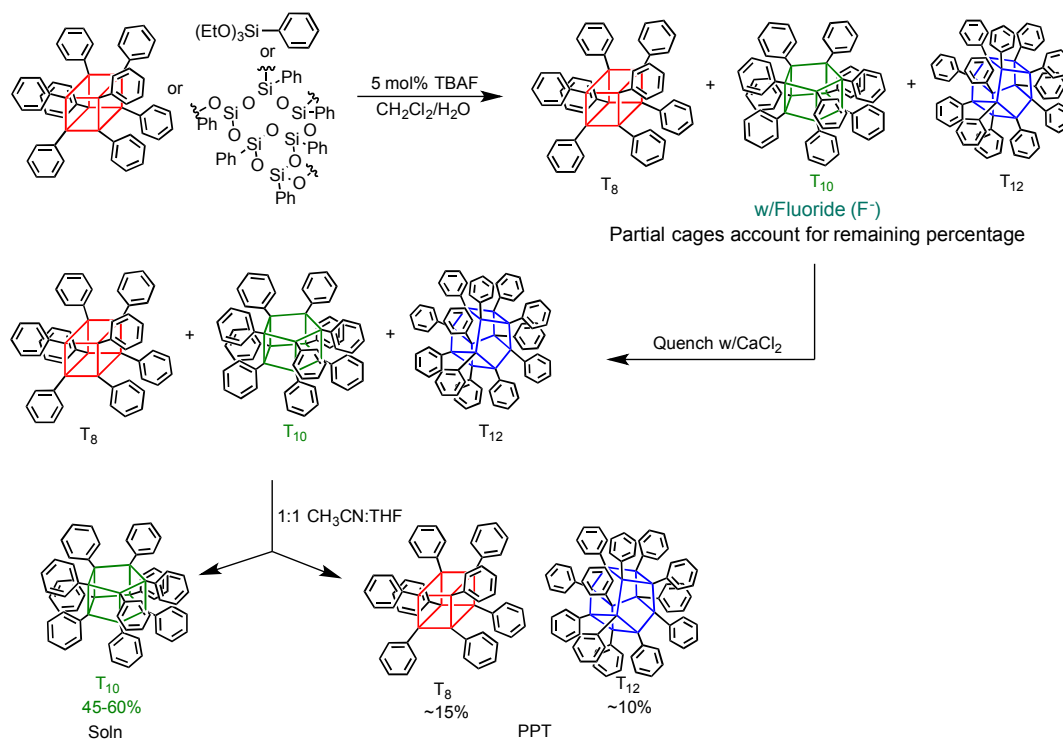
**Scheme 2**. Synthesis and separation of phenylSQs by the CaCl$_2$ quenching method.

Kawakami et al. reported that the individual cages could be separated from the mixture [4-TMS-PhSiO$_{1.5}$]$_{8,10,12}$ using selective solubility/crystallization providing the point of entrée for our studies. We explored single and double component solvent systems (i.e. acetonitrile, ethyl-acetate, etc) finding that mixtures of THF/acetonitrile or ethyl-acetate/acetonitrile permit effective separation.[33,55] A 1:1 or 1:1.2 mixture of THF:acetonitrile solubilizes the T$_{10}$ cage to the exclusion of the T$_8$ and T$_{12}$ cages, which can be filtered off as white powder. The 1:1.2 solvent mixture gives purer T$_{10}$, but at a lower yield (~40 %). Note that the T$_8$ and T$_{12}$ mixture can be recycled through re-equilibration to give more [PhSiO$_{1.5}$]$_{10}$.

The dissolved T$_{10}$ is then concentrated and added to methanol to initiate precipitation and isolated by filtration. This reaction system typically gives T$_{10}$ yields of 45-60%, with the remaining products made up of partial cages, T$_8$, T$_{12}$, and <1% larger cage, at scales achieving 8.2 g (see experimental). A short silica column (2:1 hexanes:methylene chloride) allows removal of small amounts of partial cage byproducts (~2-5%).
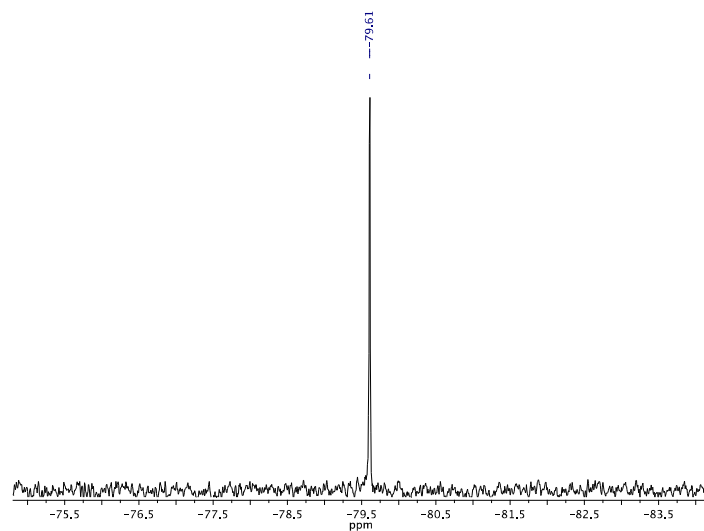
Figure **1** shows the MALDI-ToF of [PhSiO$_{1.5}$]$_{10}$ after purification [1399.8 m/z Ag$^+$-Si$_{10}$O$_{15}$(C$_6$H$_5$)$_{10}$]. Figure **2** provides the ^{29}Si NMR showing a single peak at -79.61 ppm. TGA of
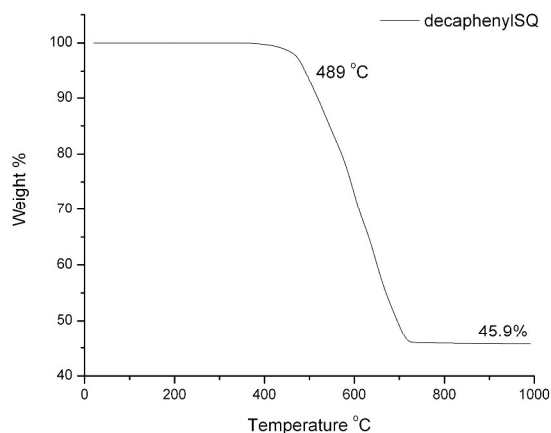
[PhSiO$_{1.5}$]$_{10}$ gives a ceramic yield of 45.9%, vs. 46.1% (theory) per Figure **3** and a T$_{d5\%}$ of 490 °C.
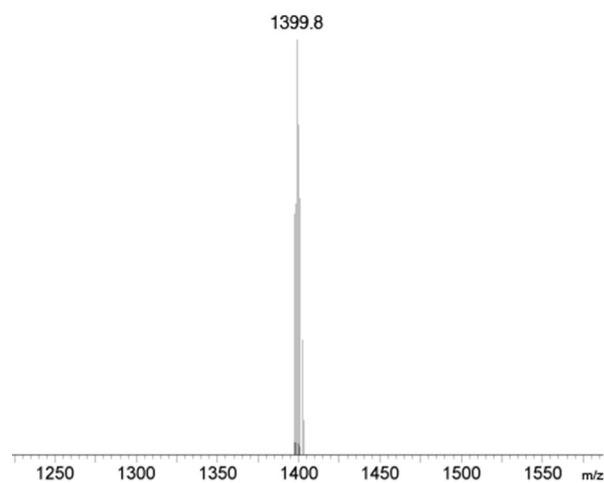
Figure 1. MALDI-ToF spectrum of [PhSiO$_{1.5}$]$_{10}$ (Phenyl T$_{10}$), Ag$^+$ peak at 1399.8 m/z [Ag-Si$_{10}$O$_{15}$(C$_6$H$_5$)$_{10}$].

Figure 2. ^{29}Si NMR of [PhSiO$_{1.5}$]$_{10}$, peak at -79.61 ppm.

8

Figure 3. TGA of $[PhSiO_{1.5}]_{10}$ in (air/10°C/min), actual and theoretical ceramic yields are 45.9% and 46.4%, with $T_{d5\%}$ of 490 °C.

The larger cages $[PhSiO_{1.5}]_{18,20,22}$, also likely equilibration products, can be separated in small quantities from $[PhSiO_{1.5}]_{10}$ using a 2:1 hexane:methylene chloride solvent system eluted through a silica column. Thus, 1 g of T_{10} provides 30 – 50 mg of the larger cages (~4%). Figure **S2** shows the MALDI-ToF of the isolated $[PhSiO_{1.5}]_{18,20,22}$ mixture.

Reaction Mechanism Studies

As noted above, one objective of these studies was to decipher, at least qualitatively, the equilibria involved in F^- promoted rearrangement reactions. The PhSQ system is used for this analysis due to its facile rearrangement with F^-, isolable products, and ease of ionization in MALDI-ToF of full and partial cages.

$[PhSiO_{1.5}]_8$, octaphenylsilsesquioxane (OPS) was chosen as the model starting material as it is a well defined structure. Note $[PhSiO_{1.5}]_{10}$ or $[PhSiO_{1.5}]_{12}$ could also have been used since equilibration of these cages results in similar product ratios (Figures **S3** and **S4**), but since we are interested in forming $[PhSiO_{1.5}]_{10}$ it makes more sense to study the equilibria involved starting from readily available $[PhSiO_{1.5}]_8$.

Reaction progress was monitored using MALDI-ToF and ^{19}F NMR. MALDI-ToF allows rapid identification of reaction intermediates and relative compositions (assuming intensities are close to quantitative), because it gives a clear indication by the mass of each species present, with intensities being proportional to its solution concentration.[32] MALDI-ToF is particularly useful for time dependent studies, since the rearrangement reactions cease in the solid state after spotting on a MALDI analysis plate. Our data suggests that similarly functionalized species ex-

hibit similar degrees of ionization; thus the peak intensities permit qualitatively if not quantitative characterization of the ratios of individual species.[32] ^{19}F NMR permits observation of Si-F species in the reaction mixture.

In the Figure **4** ^{19}F NMR study at 0 °C (standard 60 mM OPS in DCM/5 mol% F[-]) only one peak, at -130 ppm, changes intensity. We suggest that this peak corresponds to a free corner possibly Ph-O_2Si-F, or PhSiF$_3$ both of which are observed at -136 to -140 ppm range (Table **S1**).[56-60] Slight shifts of $\leq$ 10 ppm arise as a function of solvent and/or the exchange of F with O atoms. The peak at -111 ppm is one of several possible species, including pentacoordinate silicates (e.g. PhSiF$_4$[-] literature at -118.7 ppm) or fluorobenzene arising via cleavage of the Si-C bond (-113.15 ppm),[61] or possibly F[-] @[PhSiO$_{1.5}$]$_{10}$. F[-]@[RSiO$_{1.5}$]$_{10}$ has never been observed experimentally, but the computationally determined chemical shift is -112.6 ppm.[62] This value is close to the -111 ppm peak observed, however the calculated value for F[-]@[PhSiO$_{1.5}$]$_8$ is -26 vs -38 ppm found, thus, we must be cautious in assigning this value as suggested (Figure **S5**). The -123 ppm peak is from the TBAF (F[-]). The peak at -155 ppm is attributed to HF$_2$[-] (-149.5 ppm literature),[60] known to exist in TBAF mixtures due to deprotonation of water, coincidentally forming [-]OH. This species is in relatively small quantity to the TBAF F[-] ion at -123.11 ppm.[63]

In another ^{19}F NMR study (Figure **S6**) we looked at the reaction mixture 5 min after F[-] introduction at -20 °C. Two additional peaks that are observed at -145.1 and -64.8 ppm likely corresponding to a PhSiO$_2$F derivative (Table S**1**) and [PhSiO$_{1.5}$]$_{10}$[F[-]] or [PhSiO$_{1.5}$]$_8$[F[-]] derivatives respectively, as suggested from MALDI results discussed below. Though this technique seemed promising, the absence of definitive changes in the reaction over time limit the utility of ^{19}F NMR.
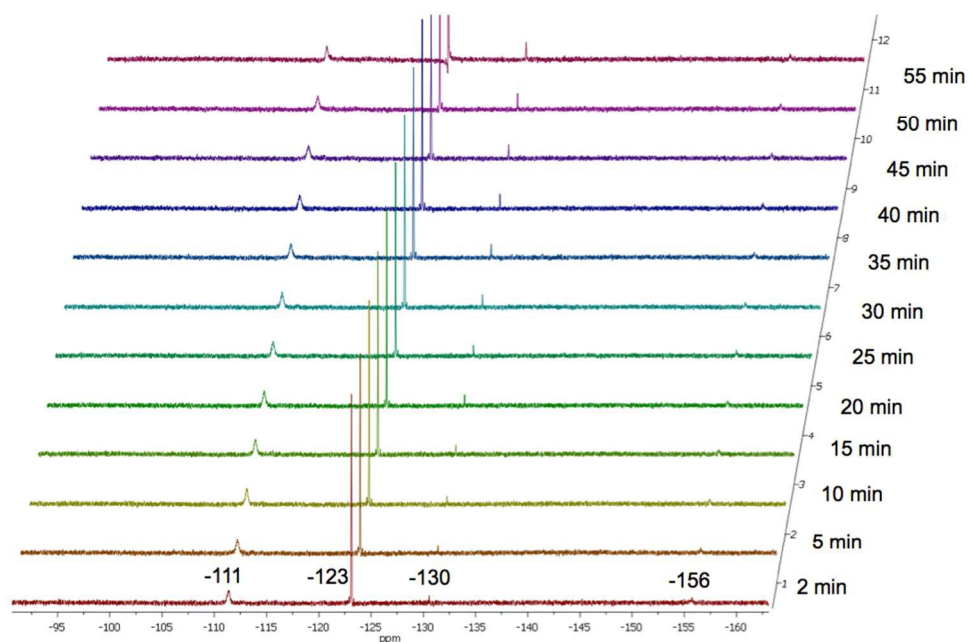
Figure 4. ^{19}F NMR reaction analysis of Reaction 3 conditions (OPS F⁻ rearrangement) over a 55 min time frame at 0 °C.

A ^{29}Si NMR study at -20 °C (12 h collection time) shows two silicon environments at -72.6 and -80.5 ppm (Figure **S7**) that could correspond to $PhSiF_3$ and $[PhSiO_{1.5}]_{10}$ respectively. The breadth and side bands of the peak at -80 ppm suggest that multiple species could be present. The literature value for $PhSiF_3$ in DCM is -72.6 ppm.[54] Attempts to use ^{29}Si NMR as an analytical tool for kinetics were thwarted by the low concentrations needed to maintain complete solution as the rearrangement reactions take place (~60 mM), resulting in long acquisition times. Therefore, MALDI-ToF remains the most reliable analytical tool. Table **S2** shows all the masses found in the MALDI studies and their proposed formulas.

Table **1** shows the set of conditions used to study $[PhSiO_{1.5}]_8$ rearrangements via MALDI-ToF analysis in dichloromethane (DCM). Reaction (3) offers the best overall conditions, with MALDI-ToF yields of 68% T_{10} and isolated yields of 52% T_{10} after 48 h.

**Table 1**. Reaction condition studies in DCM, MALDI taken at 5 min intervals up to 25 min, and then taken at 24 h for final relative %T_{10} (108 mg OPS).

Rxn	[OPS] (mM)	TBAF (mol%)	Temp. (°C)	MALDI ~%T_{10}
1	60	10	20	<1
2	60	2.5	20	32
3	60	5	20	54
4	60	1	20	21
5	120	5	20	43
6	30	5	20	25

7	15	5	20	<1
8	60	7	20	21
9	180	5	20	5
10	60	5	35	4
11	60	5	0	10
12	60	5	-35	N/A*
13	60	5	-78	N/A*

* Fluoride becomes nearly unreactive below 0 °C due to insolubility.

Figures **5** and **6** show MALDI-ToF spectra for reaction (3) at 2 and 45 min. Table **2** shows the predominant species and their proposed formulae. T_{10} is observed in small amounts with various partial and fluoride intermediate cages within 2 min after initiation at RT. These intermediates appear and show reasonable intensities at the start of the reaction, followed by further distribution into more partial cages. At 45 min, T_{10} is already the dominant product at 42% relative composition by MALDI Intensities, with the next most abundant species being $[PhSiO_{1.5}]_9(OH)$, T_{10} missing a corner (Table **1**).
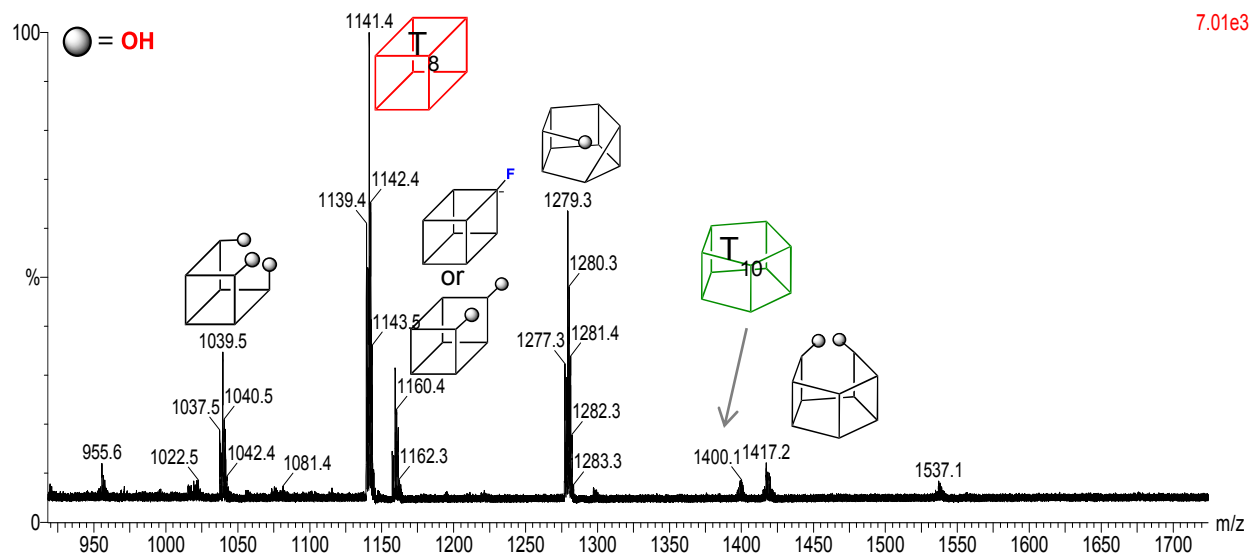
Figure 5. MALDI-ToF showing T_8 to T_{10} rearrangement reaction taken after 2 min at RT, with 1141.4 m/z T_8 and 1400.1 m/z T_{10}, Ag^+ ion peaks, phenyl groups assumed on structure corners.
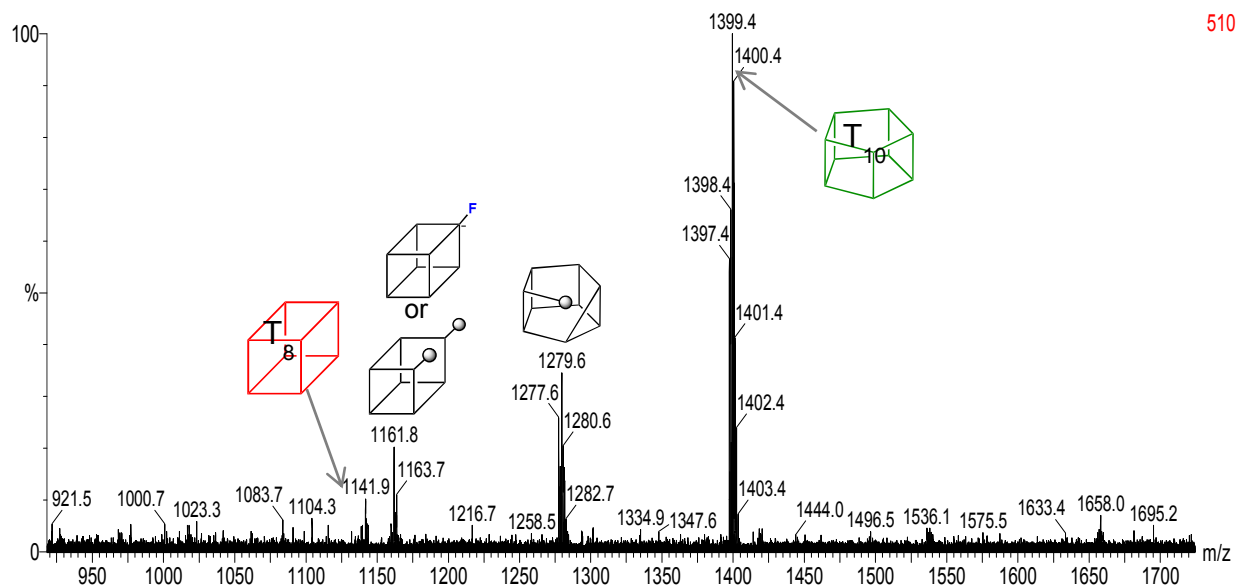
Figure 6. MALDI-ToF showing T_8 to T_{10} rearrangement reaction taken after 45 min at RT, with 1141.9 m/z T_8, 1399.4 T_{10}, and 1658 T_{12} all of which are Ag^+ ion peaks, phenyl groups assumed on structure corners.

At this point, there multiple cage sizes are present in the reaction mixture, however the $[PhSiO_{1.5}]_8$ and newly formed $[PhSiO_{1.5}]_{12}$ (1658.0 m/z) intensities are less at 45 min than after full equilibration after 1 day (Figure S1). This information suggests that quenching the reaction at 45 min would give the most easily isolable and highest yield of T_{10}, however this was not possible, likely due to the quantity of partial cages still remaining and the time it takes to quench the reaction with $CaCl_2$ (>4h).

Table 2. Observed MALDI-ToF peaks from Reaction (3) [Table 1], predicted formulae and relative peak intensities.

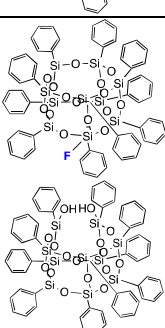| Peak Ag^+ (m/z)	Predicted formula	Proposed Structure(s)	Relative Intensity % (2 min)	Relative Intensity % (45 min)
1039.5	$[PhSiO_{1.5}]_7(OH)_3$		13	-
1141.4	$[PhSiO_{1.5}]_8$		44	3
1160.4	$[PhSiO_{1.5}]_8F$ (exo) or $[PhSiO_{1.5}]_8(OH)_2$		11	12
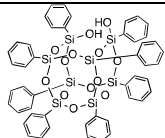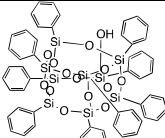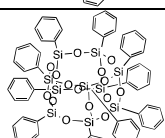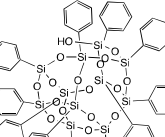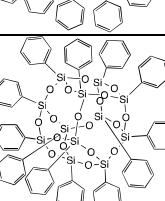
1279.3	$[PhSiO_{1.5}]_9(OH)$		27	21
1400.1	$[PhSiO_{1.5}]_{10}$		1	42
1417.2	$[PhSiO_{1.5}]_{10}F$ (exo) or $[PhSiO_{1.5}]_{10}(OH)_2$		2	-
1537.1	$[PhSiO_{1.5}]_{11}(OH)$		1	2
1658.0	$[PhSiO_{1.5}]_{12}$		-	3

Figure **7** plots the relative composition of T_{10} from MALDI peak intensities over 36 h per Reaction (3) conditions. After 45 min, the relative composition of T_{10} compared to other species remains fairly constant at ~42%, increasing slightly to 46% at 36 h suggesting the reaction to form T_{10} is actually complete within 45 min; however, during this 36 h period, the partial cages keep equilibrating until they are converted to full cages, giving a final ~1:3:1.3, ratio of T_8, T_{10}, T_{12}, with ~2-5% partials remaining.

Given that MALDI-ToF provides a method of analysis of intermediate formation and products, we ran time dependent studies using Table **1** reaction conditions. Note that reactions (1) and (7) give less than 1% T_{10} by MALDI-ToF even after 24 h. Figure **8** compares T_{10} composition vs time in the first 1500 seconds of reactions (2-6 and 9, in Table **1**).

14
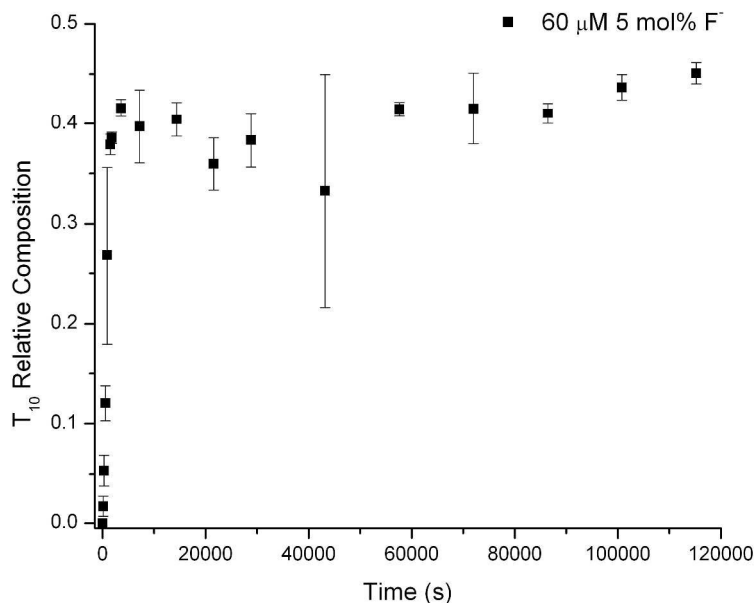
Figure 7. $[PhSiO_{1.5}]_{10}$ (1400 m/z) composition (relative intensity vs. time) over 36 h under Reaction (3) conditions (60 mM OPS in DCM, 5 mol% F⁻).

Though the peak intensities from MALDI-ToF are not ideal, clear trends are observed. First, reactions at concentrations above 120 mM or below 30 mM show decreases in T_{10} formation. Literature suggests that higher concentrations of starting materials in SQ cage formation reactions typically result in polymeric/open cages,[1-4] while lower concentrations slow intermolecular interactions decreasing reaction rates.

An alternate explanation is that increased solvation stabilizes OPS against rearrangement. Second, the addition of F⁻ above 10 mol% significantly hinders the rearrangement efficiency, likely due to increase in water concentration from added TBAF, favoring partial over fully condensed cages (see following figures). From this analysis, the best reaction concentrations to form T_{10} range from 30 to 120 mM, with F⁻ catalyst in the range of 1.5 – 7 mol%.

Figure **9** plots T_{10} formation at 0°, 20° and 35 °C over the first 1500 sec. T_{10} forms faster at 35 °C; however, the T_{10} composition falls from ~11% at 120 sec to ~1% by 1500 sec. Two explanations are possible; one is that higher temperatures stabilize partial cage intermediates, supported by the predominance of partial cages in MALDI-ToF after 10 min (Figure **S8**). Alternately, F⁻ is known to cleave Si-C bonds at ≥ 50 °C resulting in loss of R-groups.[60,64]

15
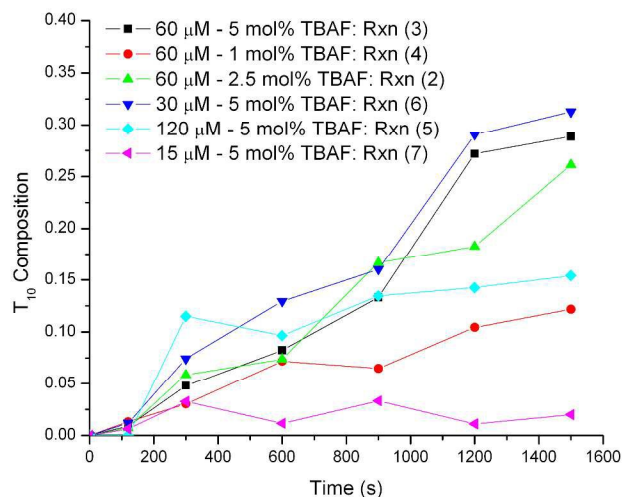
Figure 8. [PhSiO$_{1.5}$]$_{10}$ composition by MALDI within the first 1500 sec, 25 min of reactions (2-6 and 9) in Table **2**. Each data point is from an average of 30 MALDI scans.

At ≤ 0 °C, TBAF solubility drops and ice forms on the reaction surface reducing the solution water content and coincidentally rates of reaction. This results in less than 1% conversion to T$_{10}$ within 1500 sec, and only 10% conversion after 24 h. It is likely that water solvation of F$^-$ contributes to its catalytic activity.
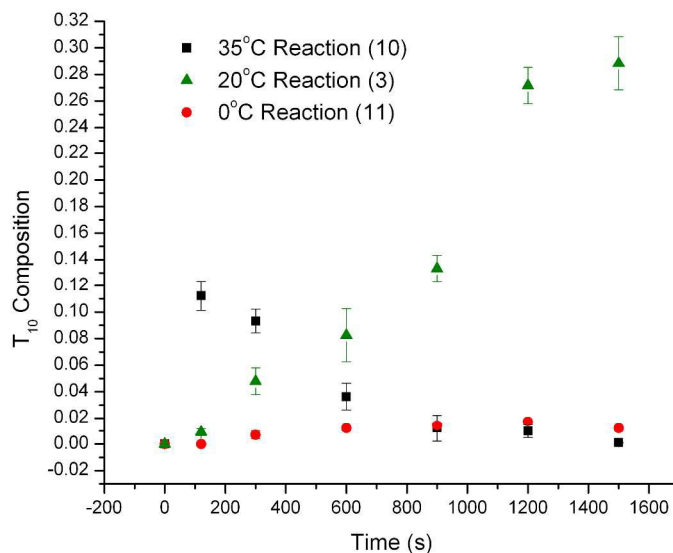
Figure 9. T$_{10}$ composition by MALDI at 0°, 20° and 35 °C for F$^-$ catalyzed rearrangement of OPS over the first 25 min of reaction (3).

We also examined solvent effects on OPS-F$^-$ rearrangement reactions (Table **3**). Likewise, reactions (14-17) explore the influence of water. In contrast, reactions (14) and (15) were run under anhydrous conditions (dry DCM, dry TBAF). The reaction (14) solution without OPS was dried for 3 h with molecular sieves to remove water from TBAF before adding OPS. After 24 h,

16

the predominant product was unexpectedly $[PhSiO_{1.5}]_{10}$. This is surprising since both Bassindale et al.[38] and Mabry and Bowers et al.[42] suggest water is necessary for rearrangement. Reaction (15) used drying conditions analogous to Bassindale et al,[38] with TBAF and distilled DCM stirred over molecular sieves/N_2/3 d, before adding oven dried OPS. The Figure **10** MALDI-ToF of this reaction shows only unreacted OPS as the predominant peak (1142.1 m/z) indicating that extensive drying is needed to remove most of the water. At this point TBAF is no longer solvated and precipitates out of solution.
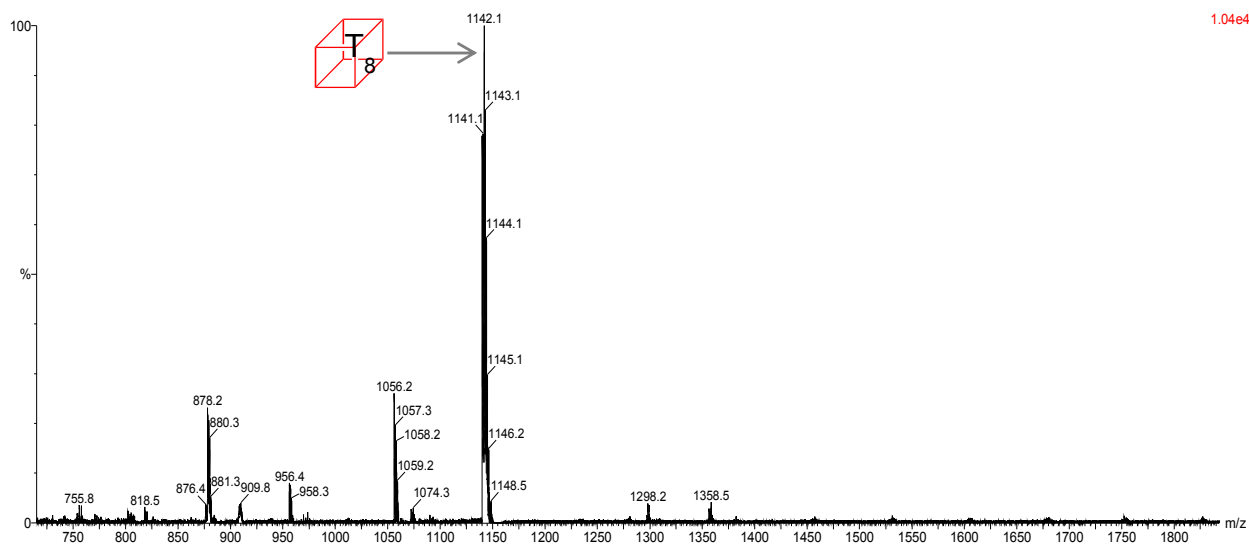
Figure 10. MALDI-ToF spectrum of OPS + TBAF in DCM under anhydrous Reaction (3) conditions (3 days drying with 4Å molecular sieves), showing OPS Ag^+ ion at 1142.1 m/z.

Reaction (15) with the 5 vol % water present in commercial 1M TBAF solutions gave the best isolated yields of $[PhSiO_{1.5}]_{10}$ of 54% (Table **1**, Reaction 3). Reaction (16), with 1 equivalent of water per cage oxygen also provided $[PhSiO_{1.5}]_{10}$ as the predominant species. Excess water [1 mL, Reaction (17)], favors partial cages, with $[PhSiO_{1.5}]_9$-$[OH]_1$-$[F]_1$ or $[PhSiO_{1.5}]_9$-$[OH]_3$ as the predominant species by MALDI at 1297.6 m/z. Both possible intermediates are within 1 amu of each other.

Table 3. OPS rearrangement studies in selected solvents without F^- removal. [60 mM concentration (108 mg of OPS in 15 mL of solvent), 20 °C/45 µL of 1 M TBAF DCM/24 h.

Rxn	Solvent	Water	Predominant Species by MALDI 24 h (m/z)
14	DCM	~0[a]	$[PhSiO_{1.5}]_{10}$ (1400.2 m/z)
15	DCM	0[b]	$[PhSiO_{1.5}]_8$ (1142.2 m/z)
15	DCM	~2.25 µL[c]	$[PhSiO_{1.5}]_{10}$ (1400.2 m/z)
16	DCM	36 µL (~1	$[PhSiO_{1.5}]_{10}$

17

		equiv)	(1400.4 m/z)
17	DCM	1 mL (excess)	$[PhSiO_{1.5}]_9\text{-}[OH]_1\text{-}[F]_1$ (1297.6 m/z)
18	DCM	2.25 µL $H_2^{18}O$	$[PhSiO_{1.5}]_8$ (1142.2 m/z)
19	Acetone	~2.25 µL	$[PhSiO_{1.5}]_8\text{-}[F]$ or $[PhSiO_{1.5}]_8\text{-}[OH]_2$ (1160.6 m/z)
20	Acetonitrile	~2.25 µL	$[PhSiO_{1.5}]_9\text{-}[OH]_1$ (1280.2 m/z)
21	DMF	~2.25 µL	$[PhSiO_{1.5}]_{10}\text{-}[F]$ or $[PhSiO_{1.5}]_{10}\text{-}[OH]_2$ (1418.0 m/z)
22	Methanol	~2.25 µL	$[PhSiO_{1.5}]_8$ (1142.4 m/z)
23	THF	~2.25 µL	$[PhSiO_{1.5}]_9\text{-}[OH]_1$ (1280.2 m/z)
24	Toluene	~2.25 µL	$[PhSiO_{1.5}]_8\text{-}[F]$ or $[PhSiO_{1.5}]_8\text{-}[OH]_2$ (1160.6 m/z)
25	1:1 THF:Acetonitrile	~2.25 µL	$[PhSiO_{1.5}]_9\text{-}[OH]_1$ (1280.2 m/z)

[a]Reaction mixture dried over 4Å molecular sieves and Na_2SO_4 for 3 h to remove water from TBAF, which was then filtered and added to a mixture of 4Å molecular sieves and OPS. [b]Reaction mixture dried over 4Å molecular sieves for 3 days under N_2 to remove water from TBAF before adding vacuum oven dried OPS. [c]1M TBAF solution contains ~5 vol% water

To fully understand the influence of water, $H_2^{18}O$ was added in place of the ~2.25 µL H_2O in TBAF [Reaction (18)] by drying the solution for 3 days as above then adding 2.25 µL of $H_2^{18}O$. The MALDI-ToF was taken after 24 h, finding that ^{18}O was incorporated into T_{10} and partial cage intermediates by their isotope patterns (1 to 14 ^{18}O atoms are observed for T_{10}, Figures **S9-S12**). The use of $H_2^{18}O$ slowed reaction rates, with T_8 still predominating after 24 h, however incorporation of ^{18}O into T_{10} shows that water is involved in the reaction mechanism, even though all required Si-O bonds are already present.

Reactions 19-25 (Table **3**) reveal solvent effects that are likely a consequence of poor OPS solubility and only soluble species are observed by MALDI-ToF.

Similar peaks are observed in most of the reactions regardless of solvent. Reaction (19) in acetone generates either $[PhSiO_{1.5}]_8\text{-}[F]$ or $[PhSiO_{1.5}]_8\text{-}[OH]_2$ (1160.6 m/z) as the major species (Figure **S13**). $[PhSiO_{1.5}]_7\text{-}[OH]\text{-}[F]$ or $[PhSiO_{1.5}]_9\text{-}[OH]_3$, $[PhSiO_{1.5}]_9\text{-}[OH]_1$ and $[PhSiO_{1.5}]_{10}\text{-}[F]$ or $[PhSiO_{1.5}]_{10}\text{-}[OH]_2$ are also observed at m/z = 1040.4, 1280.2 and 1418.6 respectively. Multiple cage structures are possible for each peak as the difference between F and OH containing structures is one proton (see Table **2**). Similar peaks are also observed in toluene and acetonitrile (Figures **S14-S15**).

In THF, $[PhSiO_{1.5}]_9\text{-}[OH]_1$ (1280.2 m/z) is the major species (see Table **3** for structures), with $[PhSiO_{1.5}]_{10}$ (1400.2 m/z) as the second most predominant species (Figure **S16**). In DMF, $[PhSiO_{1.5}]_{10}[F]/[PhSiO_{1.5}]_{10}\text{-}[OH]_2$ are the predominant species and the only solvent to show

$[PhSiO_{1.5}]_{12}[F]/[PhSiO_{1.5}]_{12}-[OH]_2$ (Figure **S17**). OPS dissolves completely in 2 min in DMF, the fastest of any solvent. In methanol (Figure **S18**), no F^- interactions were observed, and only starting OPS was seen by MALDI-ToF due to the insolubility of OPS. However, as mentioned above, no fluoride-encapsulated T_8 species were observed in the ^{19}F NMR analysis (-26 ppm). Therefore, we propose that fluoride would have to form bonds exo to the cage, initially as a pentacoordinated corner (Figure **S5**). The solvent studies did not reveal any special solvent effects that could not be attributed to poor solubility.

As part of our studies, we also attempted to characterize cage fragments to gain insight into the reaction mechanism(s). EI mass spec was taken of Reaction (3) at 2 and 5 min. Figure **11a** shows an EI mass spectrum 2 min after initiation. Both $PhSi(OH)_3$ and $PhSiF_3$ (free corners) are observed at 156.1 and 161.9 m/z respectively. Free corners $[Ag^+PhSi(OH)_2F, 266.2$ m/z] were also observed in MALDI-ToF 60 sec after adding F^- (Figure **11b**). This peak is consistent across solvent studies and has been compared to the MALDI-ToF of TBAF to verify that it is not a component of the catalyst mixture (Figure **S19**). This supports the likelihood of free cage corner transfer mechanisms theorized by Mabry and Bowers et al.[42]
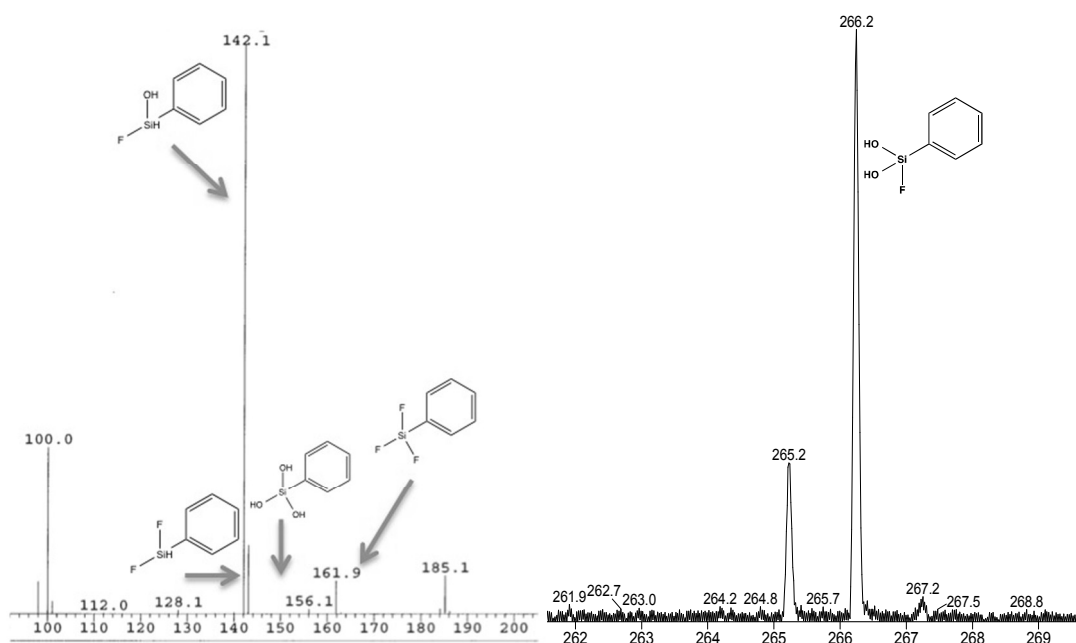
Figure 11. a. EI mass spectrum showing fluoride functionalized free corners (185.1 m/z = tributylammonium), Reaction (3) after 2 min. b. MALDI-ToF showing Ag^+ $PhSi(OH)_2F$ at 266.2 m/z, Reaction (3) after 1 min.

Mabry and Bowers et al. previously demonstrated the efficacy of TMAF (tetramethylammonium fluoride) in rearrangement.[42] Efforts to use nBu_4NX ($X = Cl^-$, Br^-) gave no reaction.[42,65]

However, the introduction of 5 mol% TBAOH w/5 vol% water using Reaction (3) conditions, promoted rearrangements forming partial cages but little T_{10} (1400 m/z) (Figure **S20**), These partial cages are similar to those seen with F^- and in polar solvent studies.

The primary products observed are $[PhSiO_{1.5}]_8$-$[OH]_2$ and $[PhSiO_{1.5}]_{10}$-$[OH]_2$ 1160 and 1418 m/z respectively, which show edge opening of both the T_8 and T_{10} cages as also seen in TBAF studies, *suggesting that partial cages with -OH are more likely than –F functionalized cages in those studies*. Other previously observed partial cage peaks present include $[PhSiO_{1.5}]_7$-$[OH]_3$ at 1040 m/z and $[PhSiO_{1.5}]_9$-$[OH]$ at 1280 m/z. The peak at 1175 m/z is $[PhSiO_{1.5}]_8$-$[OH]_4$, a likely intermediate just prior to loss of a corner in the rearrangement process.

We also followed changes in concentration of various reaction intermediates over time using Reaction (3) conditions (20 °C) plotting time vs intensities for T_{10}, T_8 and reaction intermediates per Figures **12** and **13**.

Figure **12** plots $[T_8]$ over the first 50 min of reaction revealing an exponential decay suggesting a first order dependence in $[T_8]$.[66,67] Assuming that T_8 is the sole monomer, a plot of $\ln[T_8]$ vs. time (Figure **13a**), gives a slope of (5.2×10^{-3} s^{-1}) equal to the rate of T_8 consumption.
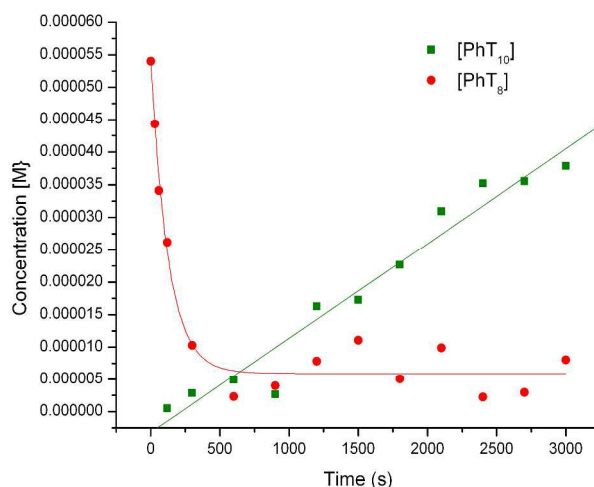
Figure 12. T_8 and T_{10} concentration vs time for Reaction (3) monitored by MALDI-ToF over the first 50 min of reaction.

The most likely first step as suggested above is attack of F^- on the T_8 cage and is supported by this plot. T_8 consumption at 35°, 0° and -35 °C can be plotted to give an activation energy (Figure **13b**, Table **5**) of ~5±1 kcal/mol for this presumed first step. The formation of pentacoordinate intermediates for both F^- and ^-OH at silicon are reported in the literature to be ~5-6 kcal/mol.[68-70] The Figure **12** plot of $[T_{10}]$ concentration over the first 50 min is linear, suggesting

the reaction is not influenced by the T_{10} concentration and T_{10} formation is not directly proportional to the consumption of T_8. This is not unreasonable if the E_a found is similar to that for formation of a pentacoordinated intermediate as a first and slow step in the rearrangement process.
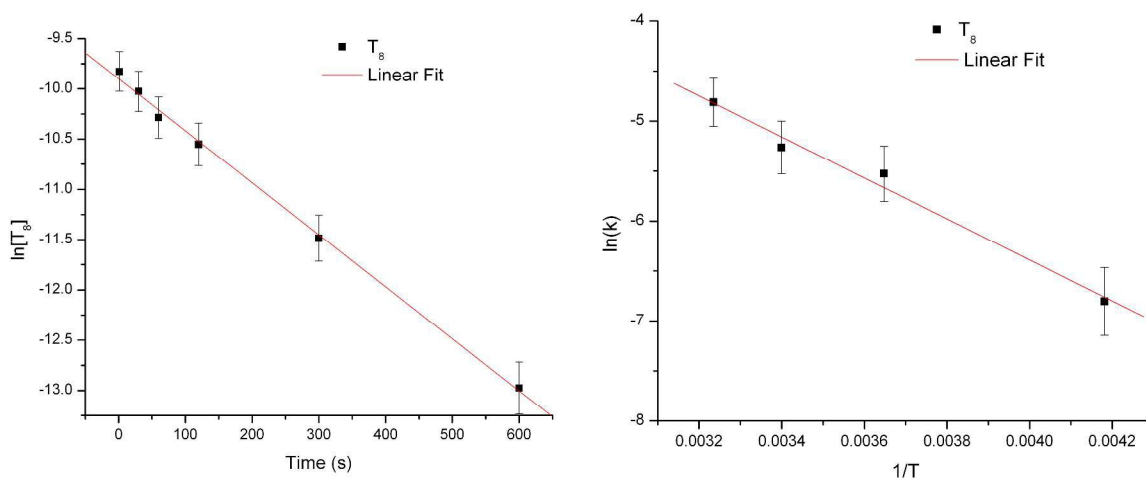
Figure 13. a. Natural log plot of T_8 concentration over the first 600 sec giving a slope of -5.2x10^{-3} s^{-1}. b. Arrhenius plot from T_8 concentrations at 35°, 20°, 0°, and -35 °C, Ea ~5±1 kcal/mol.

Table 4. Rate constants from T_8 consumption at different temperatures.

Temperature °C	k (s^{-1})
35	6.7x10^{-3}
20	5.2x10^{-3}
0	1.8x10^{-3}
-35	7x10^{-4}*

*After 25 min induction period.

Partial cage intermediates predominate after the first 600 sec of reaction. Figure **S21** uses MALDI-ToF to plot four dominant intermediates throughout the reaction. The intermediates tracked over time were inconsistent and do not permit kinetics analyses.

These studies provide a critical analysis of the rearrangement mechanism(s). First, fluoride encapsulation is not observed in ^{19}F NMR. Second, large cages ($T_{16}+$) do not appear early, thus they must form late in the process perhaps because of their higher energies (5 hartrees/Si > T_8). Third, cage fragments of 2 - 5 Si units are not seen in MALDI-ToF or EI-MS studies. Fourth, free cage corners containing both F and OH were observed early on in EI and MALDI-ToF MS, suggesting their mechanistic involvement. Fifth, TBAF solutions are known to contain four main species: $^-$OH, HF$_2$$^-$, and H$_2$O, each of these components or a combination of them could contribute to the reaction mechanism(s). Sixth, H$_2$^{18}O studies show that ^{18}O readily incorporates into the

21

T_{10} and partial cages, indicating at a minimum that free Si-OH forms and readily exchanges with water present. Given the results with TBAOH, hydroxyl groups may also participate in cage/ring-opening processes. Seventh, solvent choice greatly influences the final product ratio and composition, likely due to the difference in solubilities and stabilities of reaction intermediates. We find that dichloromethane gives the highest ratio of T_{10} and the fewest partial cages after equilibration. Eighth, $[MeSiO_{1.5}]_n$ and $[PhSiO_{1.5}]_n$ scramble with F^- to form mixed functional cages, but $[MeSiO_{1.5}]_n$ does not rearrange on its own, suggesting units from $[PhSiO_{1.5}]_n$, such as a free corner, must attack $[MeSiO_{1.5}]_n$ to insert $PhSiO_{1.5}$ to make mixed functional cages.[28] Lastly, the quenching step with $CaCl_2$ serves to remove fluoride ions to halt equilibration.

From the mass spec and NMR studies above we have proposed the structures of reaction intermediates, but we were not able to follow the changes in concentration of reaction intermediates to determine a proposed mechanism based solely on experiment, modeling studies were performed. Clearly, complex intermediates and multiple steps are involved in the reaction solutions to for $[PhSiO]_{10}$, and no one proposal is sufficiently definitive, however three plausible routes are suggested as a result of our studies.

<u>Modeling Studies</u>

$[HSiO_{1.5}]_n$ was used to model the $[PhSiO_{1.5}]_n$ systems within the Gamess computational package.[52-53] We determine the energies of the analogous $[HSiO_{1.5}]_n$ intermediates proposed above from mass spec by adapting the methods of Kudo et al who modeled T_8 cage formation from $HSi(OH)_3$.[44]

The gas phase B3LYP-6-31G(d) method was used to generate: 1. geometry optimized structures (Figure **14**); 2. thermal analysis using a double difference Hessian frequency calculations; and 3. single point energy calculations, for formation of T_8 from T_{10}. MP2 energy calculations were also performed on select systems. Table **S3** compiles energy calculations for several cage/partial cage species. In gas phase computation, T_{10} and T_{12} are both lower in total energy than T_8 by 1.6 and 1.9 kcal/mol/Si unit respectively, which is reasonable when compared to literature -0.3 and -0.5 kcal/mol respectively by Hartree Fock (HF) methods.[47,71-73] These energy values, combined with the thermal analyses were used to determine heats of reaction for conversions between intermediates (Figure **15**).
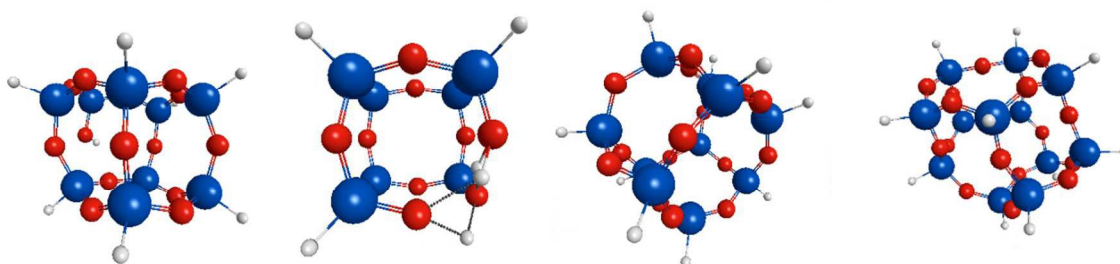
Figures 14a-d. B3LYP optimized structures: a) T_9-OH_1 b) T_7-OH_3, c) T_{10}, d) T_{12}.
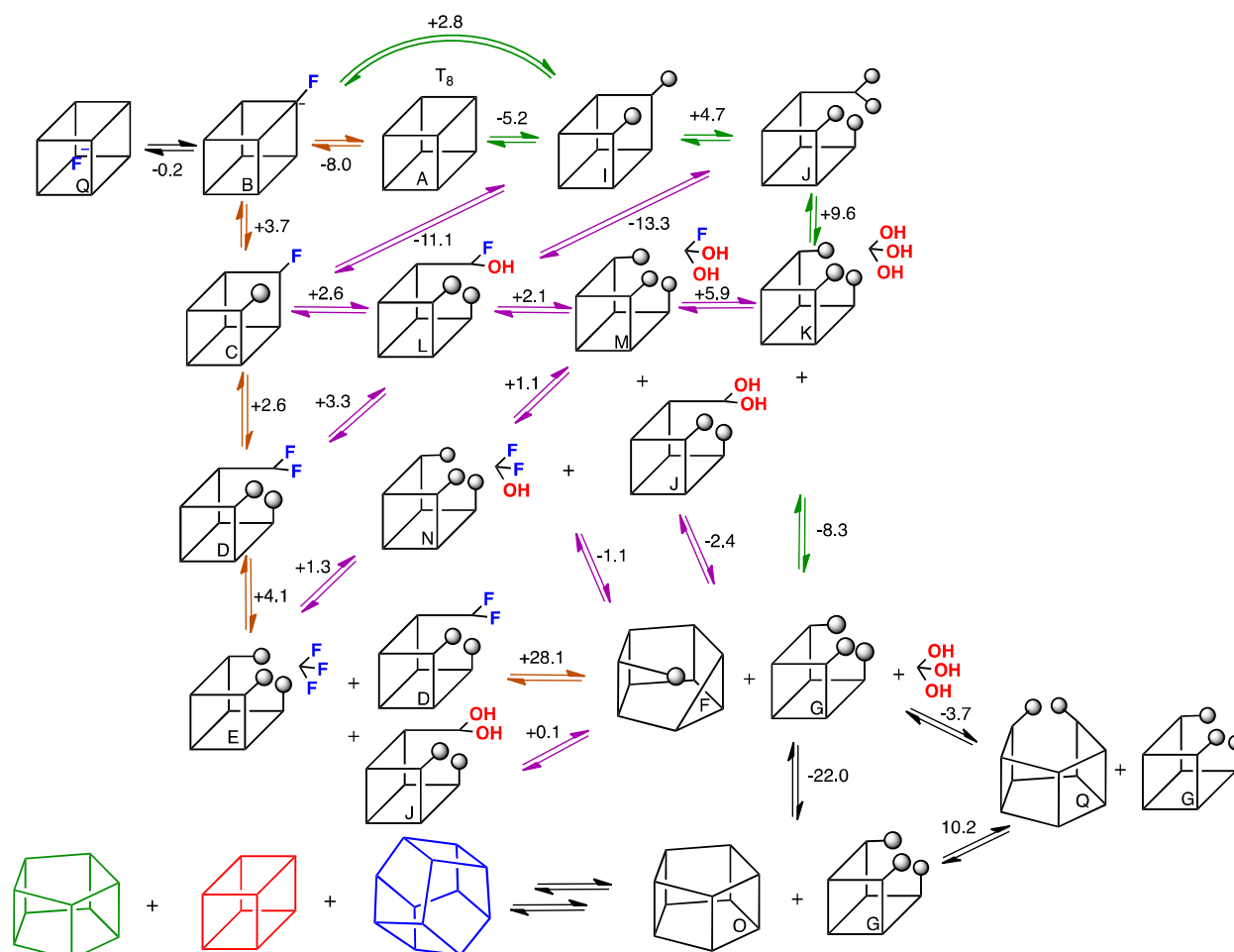
Figure 15. Potential mechanism from observed reaction intermediates and their model $[HSiO_{1.5}]_n$ heats of reaction, ΔH (kcal/mol).[*] ΔH are given on the side of the forward reaction arrow, spheres represent hydroxide capped corners, corners represent H-Si units, and lines represent oxygen bridges. Orange corresponds to F^- catalyzed pathway with net energy of 8.5 kcal/mol; Green corresponds to an ^-OH-catalyzed pathway with net energy -21.2 kcal/mol; Purple corresponds to a hybrid system $F^-/(^-OH/H_2O)$ with net energy of -24 kcal/mol.

[*]Enthalpies were used to ensure the most precise analysis, since free energies, which depend on entropies can be inconsistent due to the many vibrational and bending modes present in these molecules.

Figure **15** depicts a non-exhaustive set of potential intermediates and reaction pathways for rearrangements of T_8 to T_{10}, with formation of T_{12} likely being similar. The formation and rearrangements of SQs most certainly involve complex multiple step and multiple intermediate processes leading to complex equilibria. We describe here three reasonable pathways based on experimental analysis. The first, shown in orange, is the pure F⁻ catalyzed system, with minimal involvement of water. The first step involving the formation of F-pentacoordinated T_8 [T_8 (A) to (B)] is favored enthalpically by 8 kcal/mol. Thereafter three endothermic processes are observed in reactions (B-E), in which multiple F⁻ react to remove a cage corner. The biggest barrier (28 kcal/mol) is found for reaction (E+D to F+G); considerable energy is needed to remove F⁻ followed by replacement with ⁻OH before condensation occurs. The net reaction enthalpy for the orange pathway is 8.5 kcal/mol. If we assume structure J instead of D for this conversion, the net reaction enthalpy drops dramatically to -19.5 kcal/mol.

The green pathway depends on strong ⁻OH and H_2O interactions. The first step could consist of two possible reactions: 1. (A to B) activation of the cage by F⁻ coordination (-8.0 kcal/mol) or 2. direct attack of hydroxide (A to I). Surprisingly, both pathways are favored by the same -5.2 kcal/mol, so both are plausible. In going from (J+K to F+G to O+A) multiple intermediate steps and potential structures are possible, however few of these were repeatedly observed in our experimental studies. The net enthalpic contribution is -21.2 kcal/mol for the green pathway, which is ~30 kcal/mol lower than the orange pathway. The TBAOH catalyzed reaction studies support this pathway.

A hybrid mechanism using F⁻ with water can be proposed starting with the orange pathway (A to B to C), then following the purple arrows across (L to M) for corner removal, and then M+J through F+G to T_{10} (O). This pathway is favored by -24 kcal/mol. If the F to Q to T_{10} (O) transition is considered, the net reaction enthalpy rises to 4.5 kcal/mol. Our experimental analysis with TBAF supports the hybrid theory, since we observe mixed fluoro and hydroxyl species and ¹⁸O incorporation by mass spectrum analysis, and Si-F bonds in ¹⁹F and ²⁹Si NMR. Therefore we consider this (-24 kcal/mol) one of the most reasonable pathways.

Other possible but less likely mechanisms may also be considered. For example HF_2^- may act as a transient catalyst in these systems, even though it is not observed by MALDI-ToF. As mentioned above, large cage structures (T_{16} and larger) may act as intermediates in these reac-

tions so that T_{20} would disproportionate to two T_{10}'s. However, they are only observed late in the reaction and seem to be end products rather than intermediates.

One factor not accounted for above is the influence of solvent; in that we find that using two different solvents (THF and DCM) for Reaction (3) conditions give different equilibrium product distributions of T_8, T_{10} and T_{12} after 3 days. The explanation for changes in equilibrium may simply be attributed to the difference in solubilities of the products in different solvents. Alternately this can be thought of in terms of solvent stabilization energies. Table **S4** compares the computationally modeled solvent stabilization energies for T_8, T_{10} and T_{12} and the corresponding experimental MALDI-ToF ratios for each solvent. Though speculative, the solvent stabilization energies trend with the peak intensity ratios observed in MALDI-ToF for T_8, T_{10} and T_{12}, showing that solvent would likely influence the mechanistic pathway, stabilizing some intermediates, while destabilizing others. An important observation is that the computational methods do overestimate the favorability of T_{10} in DCM, suggesting that other influences are taking place. Verification of this will be considered in future studies.

Conclusions

We have developed a simple F⁻ catalyzed synthetic method to $[PhSiO_{1.5}]_{10}$, a molecule with the rarely observed D_{5h} structural motif. $[PhSiO_{1.5}]_{10}$ can be synthesized from any $[PhSiO_{1.5}]_n$ or $PhSi(OR)_3$ in yields up to 50% on multigram scales in CH_2Cl_2. $[PhSiO_{1.5}]_{10}$ offers a highly soluble, easily functionalized and stable 5-fold symmetric building block. We have shown in previous publications that the unique structure of stilbene/stilbenevinyl functionalized T_{10} cages offer enhanced photophysical properties such as two-photon absorption over T_8 and T_{12}. A property directly related to the polarization and charge separating ability of a system.

We have used F⁻ catalyzed rearrangement to make many SQ systems over the years, including vinyl and mixed phenyl/vinylSQs, however the process by which this occurs has eluded us. In this report we set out to solve at least qualitatively the processes involved in this rearrangement process, specifically for the conversion of $[PhSiO_{1.5}]_8$ to $[PhSiO_{1.5}]_{10}$. We have shown that the mechanism by which F⁻ catalyzed rearrangement occurs is highly complicated and involves the equilibration of many intermediates. MALDI-ToF was the most effective method for experimentally analyzing reaction progress and kinetics. We find that the activation energy for the formation of pentacoordinated F-$[PhSiO_{1.5}]_8$ is 5±1 kcal/mol, a barrier readily overcome at room

temperature, and that trace water is necessary for rearrangement to occur. With the assistance of computational modeling we proposed the three most plausible reaction pathways, finding that F⁻ catalyzed rearrangement most likely follows a hybrid mechanism involving F⁻ and water with a net enthalpic favorability of -24 kcal/mol. The mechanistic studies described here will help in the design of F⁻ catalyzed reaction conditions for favoring specific cage sizes and synthesizing other $[RSiO_{1.5}]_{10}$ derivatives.

ASSOCIATED CONTENT

Supporting Information: Additional experimental details and characterization data. This material is available free of charge via the Internet at http://pubs.acs.org.

AUTHOR INFORMATION

Corresponding Authors
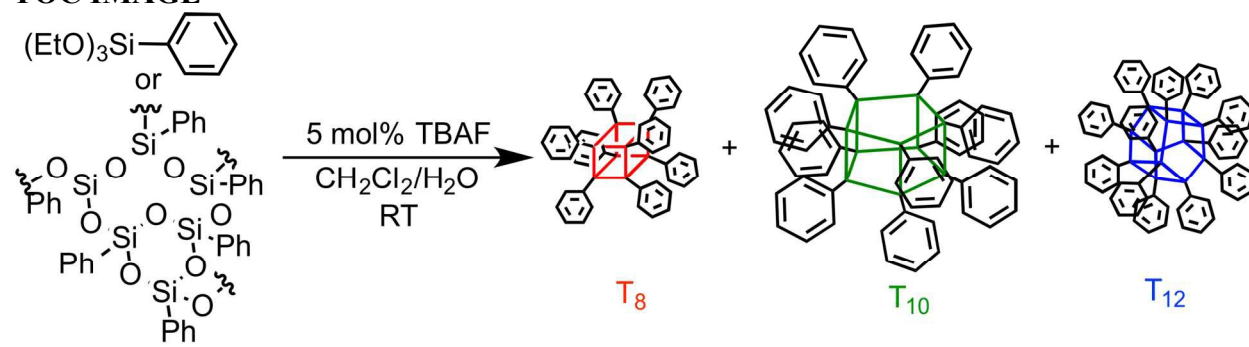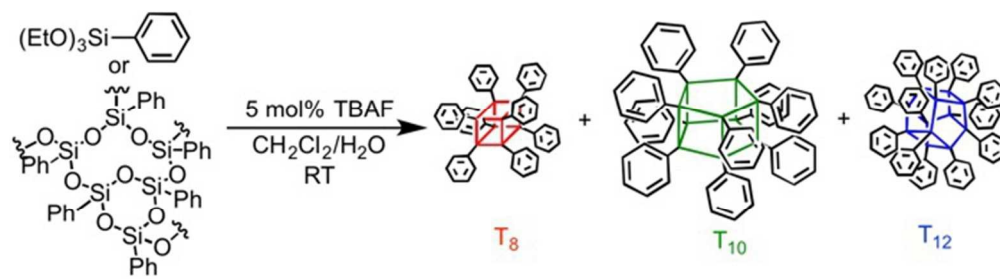*talsdad@umich.edu, tgoodson@umich.edu

ACKNOWLEDGMENT

REFERENCES

1. M. Voronkov, V. Lavrent'yev, *Top. Curr. Chem.* 1982, **102**, 199–236.
2. R. H. Baney, M. Itoh, A. Sakakibara, T. Suzuki, *Chem. Rev.* 1995, *95*, 1409–1430.
3. D. Loy, K. Shea, *Chem. Rev.* 1995, **95**, 1431–1442.
4. G. Calzaferri, "Silsesquioxanes," in Tailor-made Silicon-Oxygen Compounds, from molecules to materials, R. Corriu and P. Jutzi eds. Publ. Friedr. Vieweg&Sohn GmbH, Braunshweig/Weisbaden, Germany 1996, 149-169.
5. J. Lichtenhan, "Silsesquioxane-based Polymers," in Polymeric Materials Encyc., J.C. Salmone Ed. Vol. 10, CRC Press, N.Y., 1996, 7768-77.
6. A. Provatas, J. G. Matisons, *Trends Polym. Sci.* 1997, **5**, 327-33.
7. L. Wang, H. Ni, C. U. Pittman Jr, *J. Inorg. Organomet. Polym.* 2002, **11**, 123–154.
8. R. Duchateau, *Chem. Rev.* 2002, **102**, 3525–3542.
9. Y. Abe, T. Gunji, *Prog. Polym. Sci.* 2004, **29**, 149–182.
10. S. H. Phillips, T. S. Haddad, S. J. Tomczak, *Curr. Opin. Solid State Mater. Sci.* 2004, **8**, 21–29.
11. R. Y. Kannan, H. J. Salacinski, P. E. Butler, A. M. Seifalian, *Acc. Chem. Res.* 2005, **38**, 879–884.
12. R. M. Laine, *J. Mater. Chem.* 2005, **15**, 3725.
13. P. D. Lickiss, F. Rataboul, *Adv. Organomet. Chem.* 2008, **57**, 1–116.
14. K. L. Chan, P. Sonar, A. Sellinger, *J. Mater. Chem.* 2009, **19**, 9103.
15. J. Wu, P. T. Mather, *Polym. Rev.* 2009, **49**, 25–63.

16. D. B. Cordes, P. D. Lickiss, F. Rataboul, *Chem. Rev.* 2010, **110**, 2081–2173.

17. R. M. Laine, M. F. Roll, *Macromolecules* 2011, **44**, 1073–1109.

18. P. Pescarmona, T. Maschmeyer, *Aust. J. Chem.* 2001, **54**, 583–596.

19. S. Chimjarn, R. Kunthom, P. Chancharone, R. Sodkhomkhum, P. Sangtrirutnugul, V. Er-vithayasuporn, *Dalt. Trans.* 2015, **44**, 916–919.

20. V. Ervithayasuporn, S. Chimjarn, *Inorg. Chem.* 2013, **52**, 13108–13112.

21. A. S. Lee, S.-S. Choi, H. S. Lee, K.-Y. Baek, S. S. Hwang, *Dalt. Trans.* 2012, **41**, 10585.

22. Y. Kawakami, Y. Kabe, *Chem. Lett.* 2010, **39**, 1082–1083.

23. A. J. Barry, W. H. Daudt, J. J. Domicone, J. W. Gilkey, *J. Am. Chem. Soc.* 1955, **77**, 4248–4252.

24. J. F. Brown, L. H. Vogt, P. I. Prescott, *J. Am. Chem. Soc.* 1964, **86**, 1120–1125.

25. A. R. Bassindale, Z. Liu, I. A. MacKinnon, P. G. Taylor, Y. Yang, M. E. Light, P. N. Horton, M. B. Hursthouse, *Dalt. Trans.* 2003, 2945–2949.

26. M. F. Roll, J. W. Kampf, Y. Kim, E. Yi, R. M. Laine, *J. Am. Chem. Soc.* 2010, **132**, 10171–10183.

27. M. Z. Asuncion, R. M. Laine, *J. Am. Chem. Soc.* 2010, **132**, 3723–3736.

28. M. Ronchi, S. Sulaiman, N. R. Boston, R. M. Laine, *Appl. Organomet. Chem.* 2009, *24*, 551–557.

29. J.-H. Jung, R. M. Laine, *Macromolecules* 2011, **44**, 7263–7272.

30. J.-H. Jung, J. C. Furgal, T. G. Goodson III, T. Mizumo, M. Schwartz, K. Chou, J.-F. Vonet, R. M. Laine, *Chem. Mater.* 2012, **24**, 1883–1895.

31. J.-H. Jung, J. C. Furgal, S. C. Clark, M. C. Schwartz, K. Chou, R. M. Laine, *Macromolecules*, 2013, **46**, 7580-7590.

32. J. C. Furgal, J.-H. Jung, S. C. Clark, T. Goodson III, R. M. Laine, *Macromolecules* 2013, **46***, 7591-7604.

33. A. Miyazato, C. Pakjamsai, Y. Kawakami, *Dalton Trans.* 2010, **39**, 3239–3244.

34. M. F. Roll, J. W. Kampf, R. M. Laine, *Cryst. Growth Des.* 2011, **11**, 4360–4367.

35. X. Feng, S. Zhu, K. Yue, H. Su, K. Guo, C. Wesdemiotis, W.-B. Zhang, S. Z. D. Cheng, Y. Li, *ACS Macro Lett.* 2014, **3**, 900–905.

36. Bauert, T.; Merz, L.; Bandera, D.; Parschau, M.; Siegel, J. S.; Ernst, K.-H. *J. Am. Chem. Soc.* 2009, **131**, 3460–3461.

37. J.-F. Ayme, J. E. Beves, D. A. Leigh, R. T. McBurney, K. Rissanen, D. Schultz, *J. Am. Chem. Soc.* 2012, **134**, 9488–9497.

38. A. R. Bassindale, H. Chen, Z. Liu, I. A. MacKinnon, D. J. Parker, P. G. Taylor, Y. Yang, M. E. Light, P. N. Horton, M. B. Hursthouse, *J. Organomet. Chem.* 2004, **689**, 3287–3300.

39. A. R. Bassindale, M. Pourny, P. G. Taylor, M. B. Hursthouse, M. E. Light, *Angew. Chem. Int. Ed.* 2003, **115**, 3611–3614.

40. Y. El Aziz, A. R. Bassindale, P. G. Taylor, P. N. Horton, R. A. Stephenson, M. B. Hursthouse, *Organometallics* 2012, **31**, 6032–6040.

41. E. Rikowski, H. C. Marsmann, *Polyhedron* 1997, **16**, 3357–3361.

42. S. E. Anderson, D. J. Bodzin, T. S. Haddad, J. A. Boatz, J. M. Mabry, C. Mitchell, M. T. Bowers, *Chem. Mater.* 2008, **20**, 4299–4309.

43. M. Bahrami, H. Hashemi, X. Ma, J. Kieffer, R. M. Laine, *Phys. Chem. Chem. Phys.* 2014, **16**, 25760–25764.

44. T. Kudo, M. S. Gordon, *J. Am. Chem. Soc.* 1998, **120,** 11432–11438.

45. T. Kudo, M. S. Gordon, *J. Phys. Chem. A* 2000, **104**, 4058–4063.
46. T. Kudo, M. S. Gordon, *J. Phys. Chem. A* 2002, **106**, 11347–1135.
47. T. Kudo, K. Machida, M. S. Gordon, *J. Phys. Chem. A* 2005, **109**, 5424–5429.
48. S, Yamamoto, N. Yasuda, A. Ueyama, H. Adachi, M. Ishikawa, *Macromolecules* 2004, **37**, 2775–2778. □
49. R. Feher, J. J. Schwab, D. Soulivong, J. W. Ziller, *Main Group Chem.* **1997**, **2**, 123–132.
50. P. P. Pescarmona, M. E. Raimondi, J. Tetteh, B. McKay, T. Maschmeyer, *J. Phys. Chem. A* 2003, **107**, 8885–8892.
51. J. F. Brown Jr., *J. Am. Chem. Soc.* 1965, **87**, 4317–4324.
52. M. W. Schmidt, K. K. Baldridge, J. A. Boatz, S. T. Elbert, M. S. Gordon, J. H. Jensen, S. Koseki, N. Matsunaga, K. A. Nguyen, S. Su, T. L. Windus, M. Dupius, J. A. Montgomery, *J. Comput. Chem.,* 1993, **14**, 1347-1363.
53. "Advances in electronic structure theory: GAMESS a decade later" M.S. Gordon, M.W. Schmidt pp. 1167-1189, in "Theory and Applications of Computational Chemistry: the first forty years" C.E. Dykstra, G. Frenking, K.S. Kim, G.E. Scuseria (editors), Elsevier, Amsterdam, 2005.
54. Z, Li, Y. Kawakami, *Chem. Lett.* 2008, **37**, 804–805.
55. J. C. Furgal, J.-H. Jung, T. Goodson III, R. M. Laine, *J. Am. Chem. Soc.,* 2013, **135**, 12259-12269.
56. H. Lenormand, J. P. Goddard, L. Fensterbank, *Org. Lett.* 2013, **15**, 748–751.
57. F. Klanberg, E. L. Muetterties, *Inorg. Chem* 1968, **7**, 155.
58. W. B. Farnham, R. L. Harlow, *J. Am. Chem. Soc.* 1981, **15**, 4608–4610.
59. R. O. Day, C. Sreelatha, J. A. Deiters, S. E. Johnson, J. M. Holmes, L. Howe, R. R. Holmes, *Phosphorus. Sulfur. Silicon Relat. Elem.* 1995, **100**, 87–105.
60. M. G. Voronkov, E. V. Boyarkina, I. A. Gebel, A. I. Albanov, S. V. Basenko, *Russ. J. Gen. Chem.* 2005, **75**, 1927–1929.
61. J. A. Aguilar, G. A. Morris, A. M. Kenwright, *RSC Adv.* 2014, **4**, 8278.
62. J. Tossell, *J. Phys. Chem. C* 2007, **111**, 3584–3590.
63. G. Yu, Z. Zhang, C. Han, M. Xue, Q. Zhou, F. Huang, *Chem. Commun.* 2012, **48**, 2958.
64. R. M. Laine, M. Bahrami, X. Zhang, *Manuscript in Preparation.*
65. M. Ronchi, R. M. Laine, *Unpublished Results*
66. H. Cheng, R. Tamaki, R. M. Laine, F. Babonneau, Y. Chujo, Treadwell, D. R. *J. Am. Chem. Soc.* 2000, **122**, 10063–10072.
67. E. V. Anslyn, D. A. Dougherty, *Modern Physical Organic Chemistry*; J. Murdzek, Ed.; University Science Books: Sausalito, CA, 2006; pp. 355–406.
68. M. Z. Asuncion, I. Hasegawa, J. Kampf, R. M. Laine, *J. Mater. Chem.* 2005, **15**, 2114.
69. R. O. Day, C. Sreelatha, J. A. Deiters, S. E. Johnson, J. M. Holmes, L. Howe, R. R. Holmes, *Phosphorus. Sulfur. Silicon Relat. Elem.* 1995, **100**, 87–105.
70. R. K. Marat, A. F. Janzen, *Can. J. Chem.* 1977, **55**, 3845–3849.
71. K.-H. Xiang, R. Pandey, U. C. Pernisz, C. Freeman, *J. Phys. Chem. B* 1998, **102**, 8704–8711.
72. S. S. Park, C. Xiao, F. Hagelberg, D. Hossain, C. U. Pittman, S. Saebo, *J. Phys. Chem. A* 2004, **108**, 11260–11272.
73. K. Jug, I. P. Gloriozov, *Phys. Chem. Chem. Phys.* 2002, **4**, 1062–1066.

TOC IMAGE

$(EtO)_3Si$—Ph

or

$\xrightarrow{\text{5 mol\% TBAF}}$
CH$_2$Cl$_2$/H$_2$O
RT

T$_8$ + T$_{10}$ + T$_{12}$

Fluoride Catalyzed Rearrangement of $PhSiO_{1.5}$ Favoring $[PhSiO_{1.5}]_{10}$

245x97mm (72 x 72 DPI)